Article:
Rodriguez-Galeano, K.F., Nutter, J., Azakli, Y. et al. (2024) The effect of the increased strain per pass during the hot-rolling and its effect on the tensile properties of V-Mo and Cr-V-Mo microalloyed dual-phase steels. Journal of Materials Science, 59. pp. 22228-22249. ISSN: 0022-2461

https://doi.org/10.1007/s10853-024-10373-5

J Mater Sci (2024) 59:22228–22249

Metals & corrosion

The effect of the increased strain per pass during the hot-rolling and its effect on the tensile properties of V-Mo and Cr-V-Mo microalloyed dual-phase steels

Karol F. Rodriguez-Galeano[1,2,*], John Nutter[1], Yunus Azakli[1], Carl Slater[3], and W. Mark Rainforth[1,*]

[1] *Department of Materials Science and Engineering, The University of Sheffield, Sir Robert Hadfield Building, Mappin Street, Sheffield S1 3JD, UK*

[2] *TATA Steel, 1970 CA Ijmuiden, The Netherlands*

[3] *Advanced Steel Research Centre, University of Warwick, Coventry CV4 7AL, UK*

Received: 16 August 2024
Accepted: 21 October 2024
Published online: 3 December 2024

ABSTRACT

It is well known that the thermomechanical processing parameters affect the mechanical properties of dual-phase (DP) steels, but optimization still remains a key challenge. This work studied two interphase precipitation-strengthened DP steels based on V, Mo, and V, Mo, Cr microalloy additions. Hot-rolling was performed with a strain per pass of 0.2 and 0.4 before isothermal transformation at temperatures between 600 and 690 °C to determine the effect of these process parameters on microstructure, particularly interphase precipitation. The microstructure was carefully correlated with the mechanical properties. It was found that a higher strain during hot rolling increases the transformation kinetics of austenite to ferrite and also increases the volume fraction of the interphase precipitation within it, leading to higher strength values. The reaustenitization temperature before the isothermal transformation also plays an important role, with increased temperature reducing the segregation banding effect and increasing the amount of ferrite. The optimal reaustenitization temperature depends on the composition, being 1250 °C for the microalloyed steel with Cr additions and 1150 °C for the Cr-free microalloyed steel. A new method was used to calculate the yield strength of these DP microalloyed steels, including the strengthening contributors of each phase and the banding effect brought into one single expression that matches the experimental results.

Handling Editor: Sophie Primig.

Address correspondence to E-mail: kfrodriguezg@unal.edu.co; m.rainforth@sheffield.ac.uk

E-mail Addresses: j.nutter@sheffield.ac.uk; y.azakli@sheffield.ac.uk; C.D.Slater@warwick.ac.uk

https://doi.org/10.1007/s10853-024-10373-5

Introduction

Due to their cost–benefit relationship, dual-phase (DP) steels are used in automobile body applications. DP steels have an excellent combination of high strength and good formability. The DP microstructure mainly consists of a tough but ductile ferrite matrix with islands of hard martensitic islands. This combination of these two phases results in high-performance steel for the design of automobile parts, allowing the production of complex parts that require higher formability during the processing and final high strength [1–3]. DP steels can be produced by traditional processing routes and also contain limited amounts of alloying elements [4]. Furthermore, predictions for the end-use properties are difficult because of the large number of parameters that affect their mechanical properties such as the volume fraction, distribution, and carbon content of each of their phases [1, 5–9].

High-strength low-alloy (HSLA) steels are usually strengthened by solid solution hardening, grain refinement hardening, and precipitation hardening [10, 11]. Grain refinement is achieved by the detailed control of the thermomechanical processing (TMCP) schedule [12–16]. Grain size is further refined when rolling at temperatures where austenite recrystallizes. The grain refinement of austenite increases the area of total boundaries to be encountered by newly nucleated α phase during $\gamma \rightarrow \alpha$ transformation, and thus reduces this final size [17, 18]. However, if rolling is performed in the austenite non-recrystallization region, it will accumulate high dislocation density within the deformed soft and ductile austenite matrix rendering good nucleation sites for transformation to ferrite that leads itself to a fine grain size [19–21].

There have been many investigations into interphase precipitation and its relationship with tensile properties [22–25]. Interphase precipitation (IP) often leads to rows of finely spaced nano-sized carbonitrides formed during the $\gamma \rightarrow \alpha$ transformation. IP is promoted in low-alloy steels by adding low-diffusion (in iron) carbide-forming elements [6–10] that can be isothermally transformed to ferrite. Cr is one of these elements that does diffuse as fast as carbon in iron. Research on Cr additions to HSLA steels has been partially limited by the harmful effect of Cr in high-strength steel welds, creating a zone of increased hardness by forming Cr carbides in the heat-affected zone which at the same time promotes the formation of martensitic-retained austenite and bainite constituents [26, 27]. Thermodynamic analysis of microalloyed steels with small Cr additions heat treated with slow cooling rates, or with an intercritical isothermal hold, revealed that Cr increases the driving force of $\gamma \rightarrow \alpha$ transformation, promoting fine grain-sized ferrite formation, and reducing IP's inter-sheet spacing, improving the tensile strength and the toughness, with a minimal reduction of elongation [28–31].

There have been numerous investigations on the effect of process route, temperature, and cooling rate on interphase precipitation of HSLA steels [32–35]. Outstanding tensile properties have been reported when warm and intercritical rolling is used, which results in important changes to the microstructure and the relationship between interphase precipitation and the tensile properties [36–38]. The interphase precipitation is controlled by four independent factors: (a) phase equilibria at the interphase, (b) interface mobility, (c) solute drag, and (d) orientation relationship (OR) between austenite and ferrite [39–42]. The theoretical and practical understanding of interphase precipitation leads to novel experiments to evaluate if changes in the steel's chemical composition or the TMCP can improve the mechanical properties and thus the application of these alloys and mechanisms [43–46]. However, there have been no studies on the relationship between the strain per pass during the hot rolling and the interphase precipitation volume and its effect on strength.

This study aims to link the variation in strengthening contributors with different strain rates during hot-rolling of V-Mo and Cr-V-Mo DP microalloyed steels. Isothermal transformation was performed on the alloys at different temperatures followed by quenching. A detailed investigation of the precipitation strengthening of the ferrite by interphase precipitation was carried out, with a comprehensive study of precipitate composition, size and volume fraction as a function of strain per pass during hot-rolling. This is associated with the mechanical behavior of microalloyed DP steels and its effect on the development of a dual-phase (DP) structure and strengths contributions from each phase.

Experimental procedure

Material

The designed alloys with chemical compositions (wt. %) given in Table 1, were vacuum-induction melted (VIM) in a Consarc VIM and cast into ~ 5 kg ingots of 80 mm × 80 mm × 100 mm. After the border removal, the ingots were cut in half to dimensions of 80 mm × 80 mm × 40 mm, they were homogenized at 1250 °C for two hours. Two different rolling schedules were performed as shown in Table 2 and then air-cooled to room temperature. Rolling was performed on a two-high Fenn (Model 081) 136 tonne rolling mill. The rolled plates were cut in two types of samples: 20 mm × 20 mm × the plate thickness (from the midsection of the plate); these samples were heated to temperatures between 1000 and 1300 °C for 30 min, and the prior-austenite grain size was measured after cooling. Samples of 150 mm × 15 mm × the plate thickness were cut along the rolling directions for dilatometry experiments. The tensile properties, the IP volume fraction and distribution were measured in the two alloys for a strain of 0.2 per hot-rolling pass in a former investigation, which is reproduced here [23].

To generate interphase precipitation, the dilatometry samples were first reheated to the maximum temperature below the onset of austenite abnormal grain growth (1245 °C) for 30 min followed by water quenching, which allowed control of the prior-austenite grain size before isothermal transformation. These samples were reheated, using a Dilatronic dilatometer, to the austenitization temperature for 3 min, cooled to the isothermal transformation temperature at a cooling rate of 10 °C/s, and held at that temperature for 90 min and then water quenched to room temperature (Fig. 1).

Dilatometer samples of steels 0.2HR and 0.2HR + Cr were reaustenitized at 1200 °C for 3 min and cooled to the isothermal transformation temperature (T_{iso}) at a rate of 10 °C/s^{-1}, held for 90 min and followed by water quenching to room temperature. The isothermal transformation was carried out at temperatures between 600 and 675 °C. Dilatometry of steels 0.4HR and 0.4HR + Cr was performed by varying the reaustenitization temperature in the range of 900 °C-1245°C, followed by cooling at a rate of 10 °C/s^{-1}, and then isothermal transformation at the temperature which was known to give the maximum ferrite fraction. The purposes of the present reaustenitization and isothermal transformation temperature changes were to understand how the transformation temperature affects interphase precipitation as well as ferrite volume fraction, and the subsequent effect on the mechanical properties of the microalloyed steels. Each procedure was replicated thrice, and the results showcased represent the mean of these repetitions.

Table 2 The initial and final thickness per pass during the hot-rolling process

Pass	Steels 0.4HR and 0.4HR + Cr		Steels 0.2HR and 0.2HR + Cr	
	Initial thickness [mm]	Final thickness [mm]	Initial thickness [mm]	Final thickness [mm]
1st	40	24	40	34.2
2nd	24	15	34.2	28.4
3rd	15	9	28.4	22.6
4th	9	7.5	22.6	16.8
5th	–	–	16.8	11

Prior-austenite grain size, ferrite volume fraction and grain size, and tensile properties

To determine the temperature for the austenite abnormal grain growth, samples of 20 mm × 20 mm × thickness of the plate were cut from the midsection of the hot-rolled plates and reheated in a tube furnace to temperatures in the range of 1000–1300 °C for 30 min. The samples were cut into two and prepared using conventional metallographic techniques. A 2% picral etchant [47] was used to measure the prior austenite

Table 1 Chemical composition of the alloys produced for this study (wt%)

	C	Mn	Si	Al	V	Mo	Cr	N
0.2HR	0.13	1.56	0.19	< 0.005	0.21	0.5	–	–
0.2HR + Cr	0.12	1.41	0.21	< 0.005	0.2	0.48	0.51	–
0.4HR	0.12	1.11	0.23	< 0.01	0.2	0.47	0.01	< 0.003
0.4HR + Cr	0.1	1.3	0.22	< 0.01	0.2	0.47	0.51	< 0.003

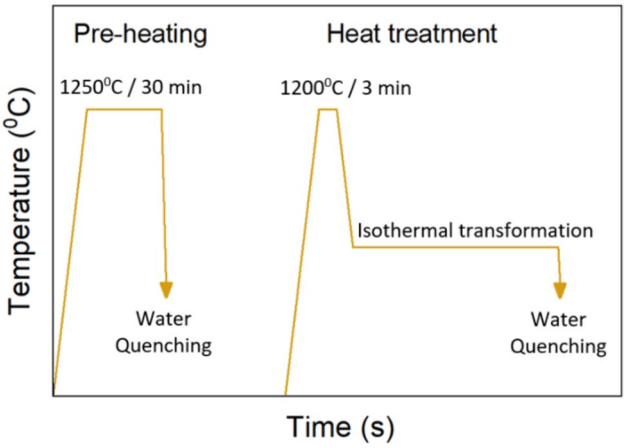

Figure 1 Scheme of the thermomechanical cycle used for each steel and condition.

grain size, using the linear intercept method (ASTM E-112) with the assistance of ImageJ software.

Samples for both metallography and tensile tests were obtained from the dilatometer samples. Samples were extracted from a 5-mm radius around the orifice where the thermocouple was positioned to ensure that the thermal history of the sample was precisely known. Metallographic samples were prepared following standard procedures and etched in a 2% nital solution for 8-12 s. The ferrite volume fraction was determined by point counting but its grain size, by the linear intercept method (ASTM E-112), all measured with the software ImageJ. Tensile samples were mechanized after the metallographic examination of each sample, verifying the structure was homogeneous along the gauge section. Three tensile samples were manufactured for each treatment. All the tensile samples were taken along the rolling direction with a gauge section of $2 \times 2.4 \times 11$ mm, which is the dimensional relationship recommended by Great Britain's standard $L_0/\sqrt{A_0} = 5$, achieving more cautious results of the total elongation than the suggested by the ASTM E8M. Tensile tests were accomplished on a Zwick/Roell Z050 at a strain rate of $4.0 \times 10^{-4} s^{-1}$ with a laser extensometer.

Precipitate analysis

The transmission electron microscopy (TEM) was conducted to analyze and quantify the amount of interphase precipitation. Volume fraction and size distribution of the precipitates were measured via carbon extraction replicas analysis. Previous work [22, 23] had shown that the size and distribution of precipitates observed in carbon extraction replicas closely matched those from STEM images of thin foil samples, considering experimental error. For thin foil samples for TEM, slices were cut from the optical metallographic specimens, mechanically thinned to 100 μm, and then electropolished using a solution consisting of 5% perchloric acid, 35% butoxyethanol, and 60% methanol. The carbon extraction replicas followed the standard procedure, involving light etching with a 2% nital solution, followed by a 7-nm thickness carbon deposition using a Quorum Q150T ES plus coater. A 10% nital solution was used for the final release of the replica. All TEM samples were examined using a JEOL JEM F200 operating at 200 kV. Particle diameter and interphase precipitation volume fraction were calculated for each sample by counting of more than 2000 particles per sample with ImageJ software.

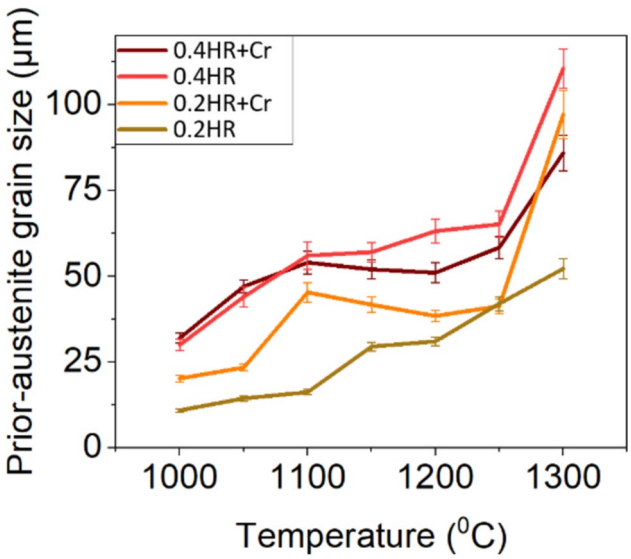

Figure 2 Average prior-austenite grain size as a function of the temperature of the two steels with different strains per pass during the hot rolling.

Results

Prior austenite grain size

After the pre-heating process, no elongated prior austenitic grains were found. Figure 2 shows the average

values of the measured prior austenite grain sizes. Lower values were obtained in the steels with 0.2 strain per hot-rolling pass. The grain size/temperature behavior was investigated to obtain the optimal austenite grain size for ferrite formation, and the re-heating temperature of it. Abnormal austenite grain growth was first observed at 1250 °C in all steels. It has been reported that smaller austenite leads to a greater ferrite formation because of the increased number of nuclei formed on the austenite grain boundaries [48–50], but this was not observed here, as shown later. The ferrite nucleation rate also depends on the steel chemistry, re-heating temperature, and time [51–54].

Microstructure

The optical micrographs shown in Figs. 3, 4, 5 and 6 were taken from dilatometer specimens, from a zone within 5 mm from where the thermocouple for the temperature control was placed. The white etched phase is ferrite nucleated and grown during the isothermal transformation, and the dark etched phase is martensite.

Figure 3 shows the 0.2HR steel isothermally transformed at a lower range of temperatures. The fraction of martensite reduces and the fraction of polygonal ferrite increases as the T_{iso} increases. The maximum amount of ferrite was found at T_{iso}≈650 °C, mostly with a polygonal morphology. For T_{iso} above 650 °C, the ferrite fraction reduces and the banding effect increases.

The microstructure of the steel 0.2HR + Cr isothermally transformed in a range of 640–675 °C is presented in Fig. 4. This structure is composed of polygonal ferrite, Widmanstätten ferrite (with its characteristic shape), and martensite. This steel showed a maximum amount of ferrite at T_{iso}≈660 °C.

Both 0.4HR and 0.4HR + Cr were isothermally transformed at 650–660 °C and 660–680 °C respectively, but with different reaustenitization temperatures (900, 1100, and 1245 °C). It is observed that the microstructure is composed also of polygonal ferrite and martensite, but with a reduced banding (Figs. 5 and 6).

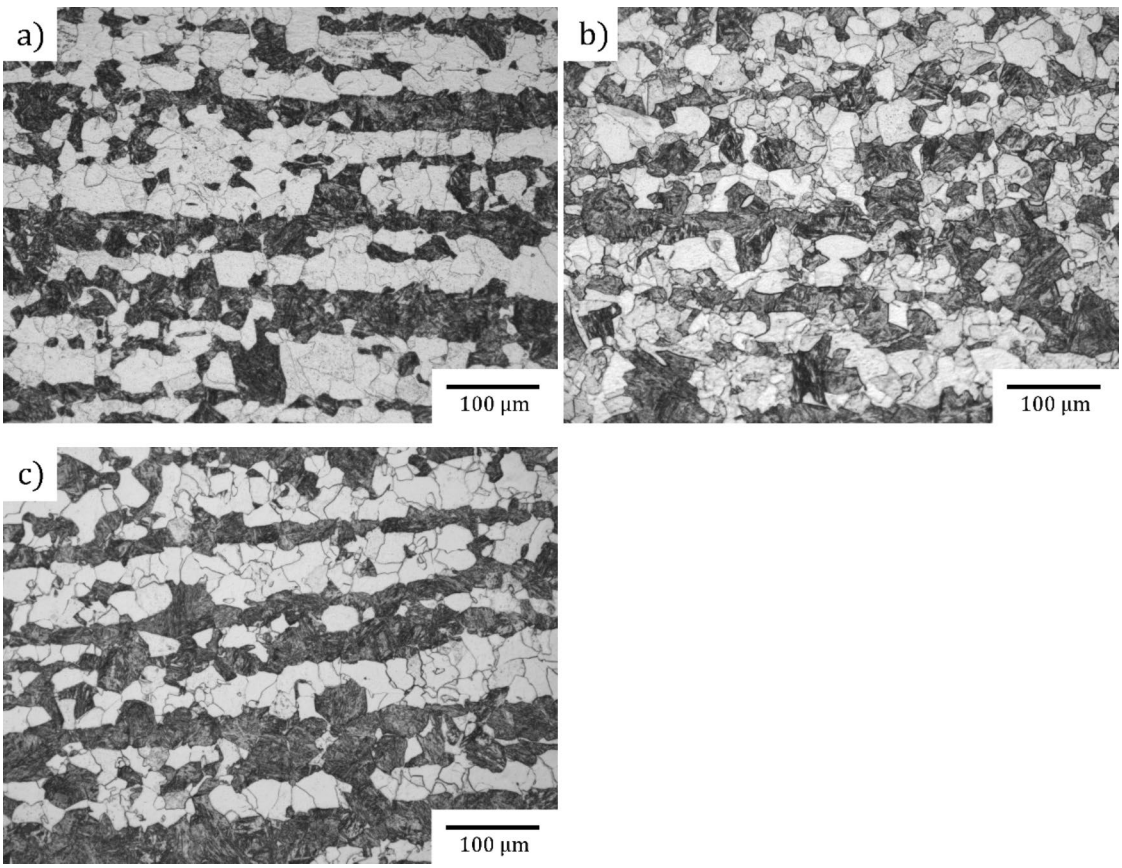

Figure 3 Optical micrographs taken from samples of the steel 0.2HR Isothermally transformed at: **a** 600 °C, **b** 655 °C, **c** 670 °C.

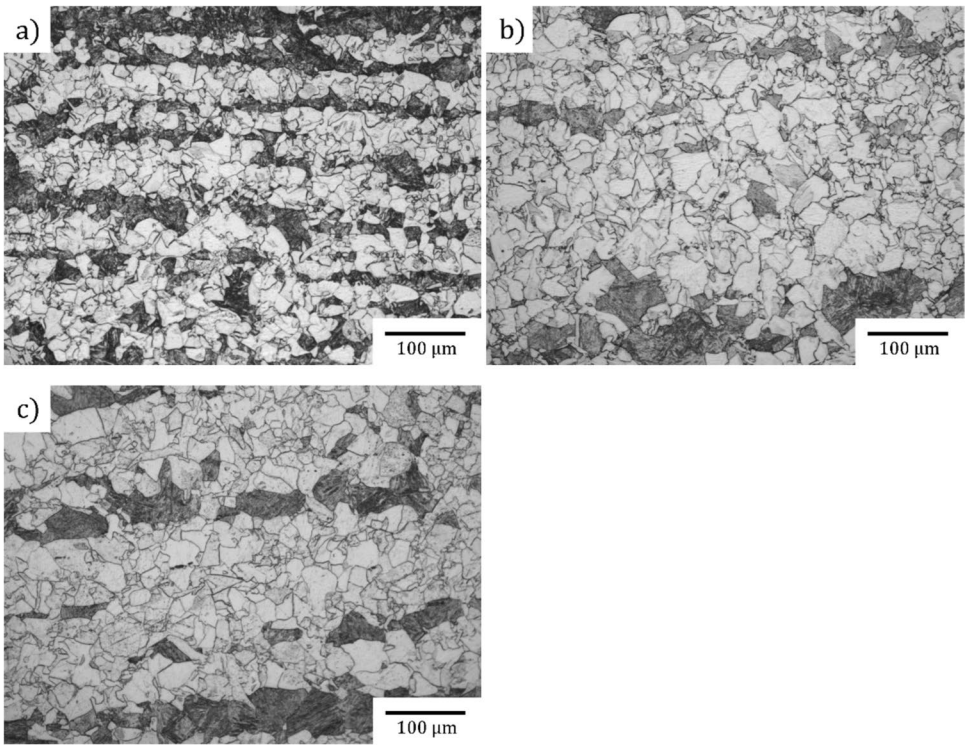

Figure 4 Optical micrographs taken from samples of the steel 0.2HR + Cr Isothermally transformed **a** 640 °C, **b** 665 °C, and **c** 670 °C.

Ferrite grain size and volume fraction are presented in Figs. 7 and 8. For the steels with 0.2 strain per pass, the fraction of total ferrite in the Cr-free steel increased as the isothermal transformation temperature was increased above 600 °C, reaching a maximum at approximately 655 °C, and then decreasing at higher temperatures. The transformation from 650 to 670 °C produced a lower volume fraction of polygonal ferrite when compared with the microalloyed with the addition of Cr. Similarly, the Cr-added steel displayed a similar trend, but with a peak ferrite content approximately 17% higher than that of the Cr-free steel, occurring at 665 °C (as shown in Fig. 7a)). Figure 7b shows that in the steels with 0.4 strain per hot-rolling pass the ferrite volume fraction changes with the reaustenitization temperature before the isothermal transformation. In the V-Mo steel, the reaustenitization at 900 °C produced ~ 15% less ferrite content than the same steel reaustenitized at 1150 and 1245 °C. In the case of the Cr containing steel, the difference in the ferrite volume fraction is irrelevant between the steels reaustenitized at 900 and 1150 °C, but around 2.5% higher for the samples reaustenitized at 1245 °C. Furthermore, the ferrite volume fraction in the Cr-free steel increased by almost 20% in the V-Mo steels with 0.4 strain per hot-rolling pass than in the same steel with 0.2 strain per hot-rolling pass.

Figure 8a and b gives the average ferrite grain size of all the steels, measured as a function of isothermal soaking temperature. In steels with 0.2 strain per hot-rolling pass, there is not much difference in the grain size of the polygonal between the Cr-added and the Cr-free steels. In the steels with 0.4 strain per hot-rolling pass the ferrite grain size increases with higher reaustenitization temperatures, as expected. At the conditions that produced the maximum ferrite after transformation (reaustenitized at 1150 °C, isothermally transformed at 650 °C for the V-Mo steel, and reaustenitized at 1245 °C, isothermally transformed at 660 °C for the Cr-V-Mo steel), there is no clear difference in the ferrite grain size.

Kinetics of the phase transformation

Figures 9 and 10 show the dilatation curves of the four alloys, Fig. 9 for the alloys with a 0.2 reduction per hot-rolling pass, and Fig. 10 for the alloys with 0.4 per hot-rolling pass. In the previous study, the effect of the Cr addition on steels with 0.2 strain was discussed in detail, concluding that the Cr addition accelerates the kinetics of transformation to ferrite [23], this effect can be also seen on steels with 0.4 strain per hot-rolling pass but also observing that the increment in the strain

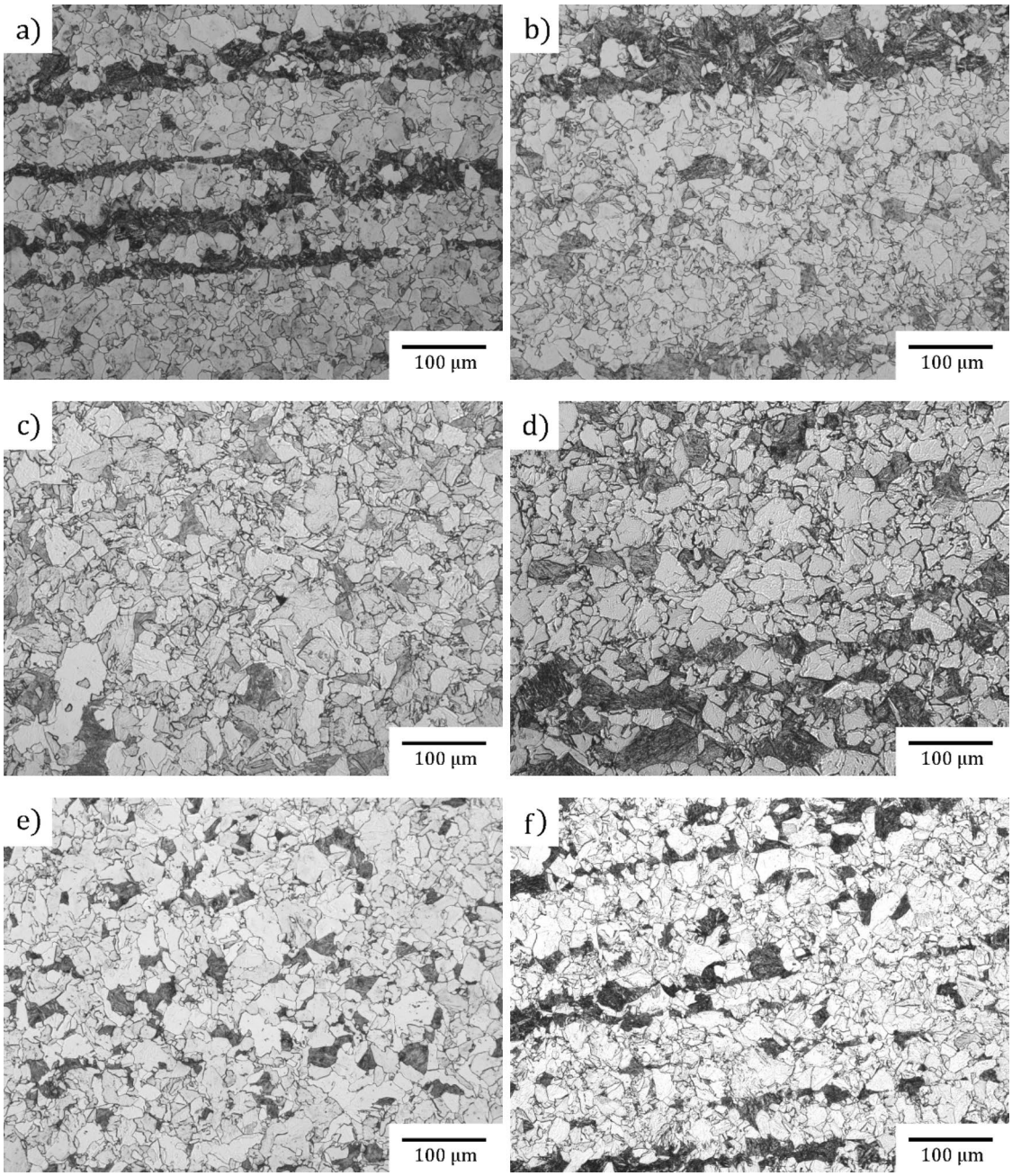

Figure 5 Microstructure of alloy 0.4HR when: **a** Reaustenitized at 900 °C and T_{iso} = 650 °C, **b** Reaustenitized at 900 °C and T_{iso} = 660 °C, **c** Reaustenitized at 1150 °C and T_{iso} = 650 °C, **d** Reaustenitized at 1150 °C and T_{iso} = 660 °C, **e** Reaustenitized at 1245 °C and T_{iso} = 650 °C, and **f** Reaustenitized at 1245 °C and T_{iso} = 660 °C.

per pass during the hot-rolling reduces the time for the $\gamma \rightarrow \alpha$ phase transformation. In addition, from the dilatometry results, it cannot be possible to conclude any effect of changing the solution annealing temperature in the range between 900 and 1245 °C on the transformation kinetics of the studied microalloyed steels.

Transmission electron microscopy

A series of TEM images taken from thin foil and carbon extraction replica specimens showing

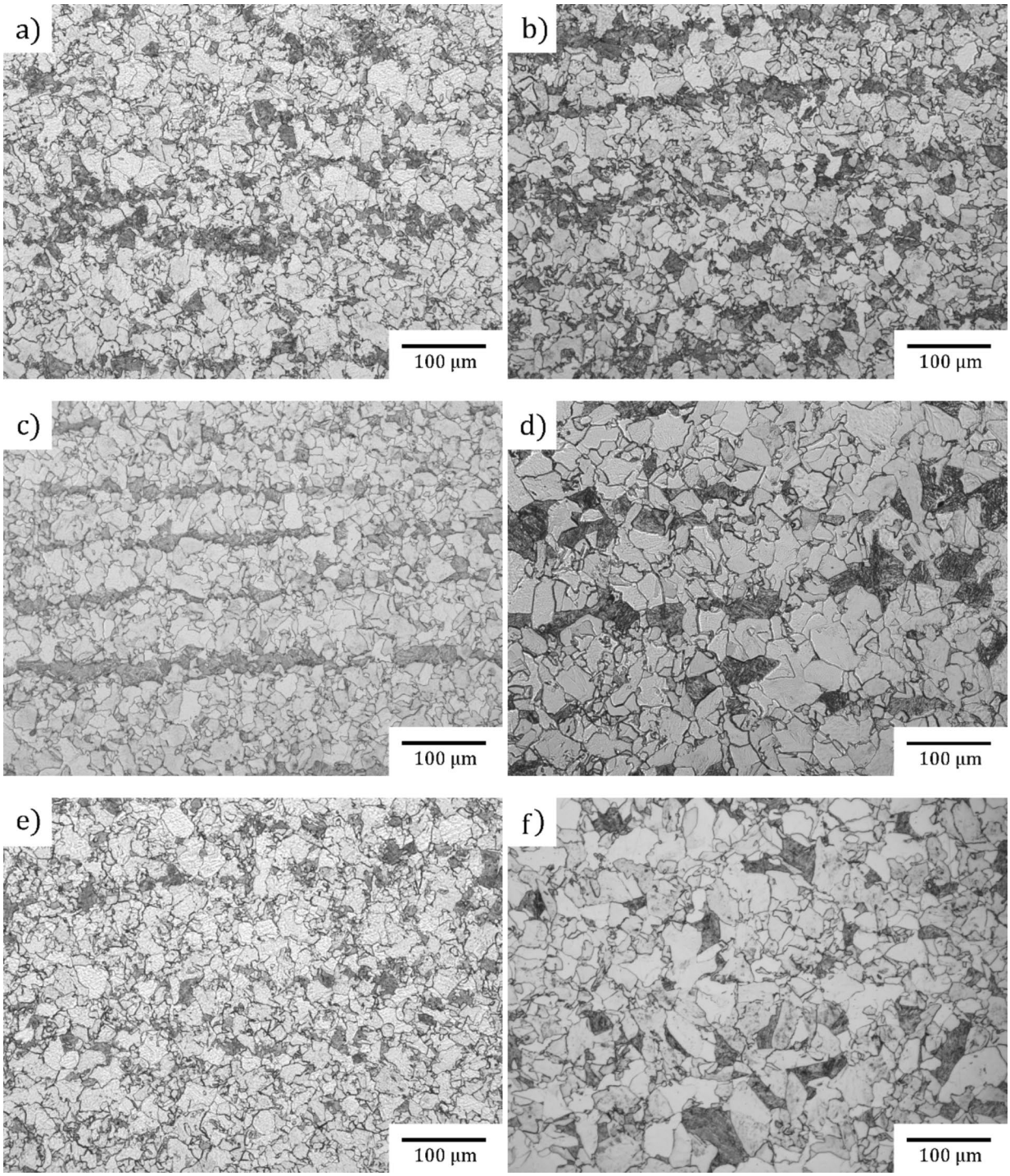

Figure 6 Microstructure of alloy 0.4HR + Cr when: **a** Reaustenitized at 900 °C and T_{iso} = 660 °C, **b** Reaustenitized at 900 °C and T_{iso} = 680 °C, **c** Reaustenitized at 1150 °C and T_{iso} = 660 °C, **d** Reaustenitized at 1150 °C and T_{iso} = 680 °C, **e** Reaustenitized at 1245 °C and T_{iso} = 660 °C, and **f** Reaustenitized at 1245 °C and T_{iso} = 680 °C.

the precipitate distribution and morphology are presented in Fig. 11. Such images show that the ferrite contains interphase precipitates with nanometre-size, with a row dispersion. Using well-defined diffraction conditions in the TEM, the inter-sheet spacing was measured for all the steels, from

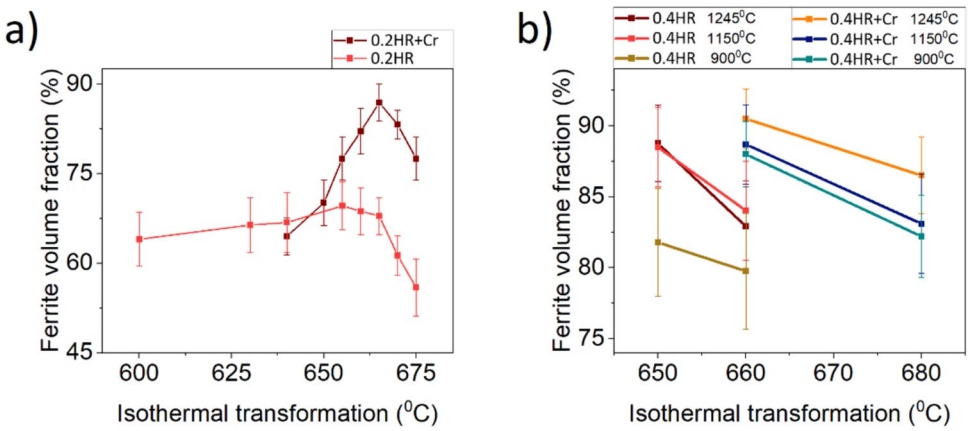

Figure 7 Average ferrite volume fraction measured from optical micrographs. **a** alloys 0.2HR, and 0.2HR + Cr, **b** alloys 0.4HR and 0.4HR + Cr. The data in a) is reproduced from ref 23.

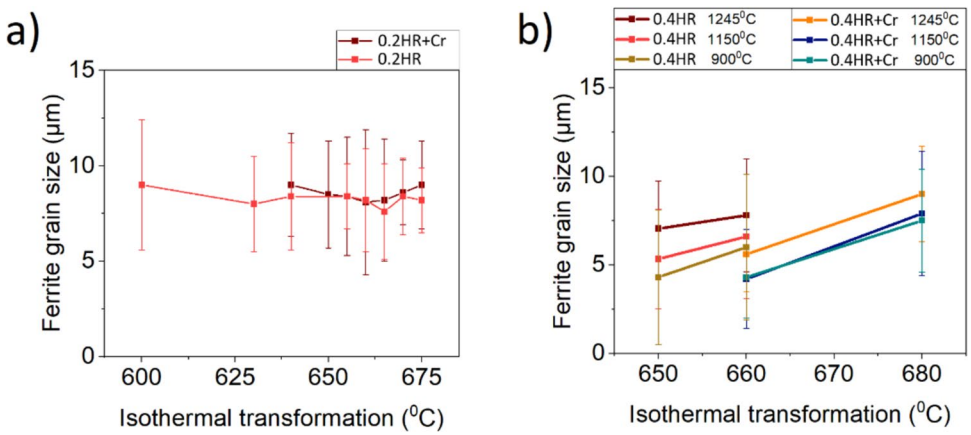

Figure 8 Average ferrite grain size measured from optical micrographs. **a** alloys 0.2HR, and 0.2HR + Cr, **b** alloys 0.4HR and 0.4HR + Cr. The data in a) is reproduced from ref 23.

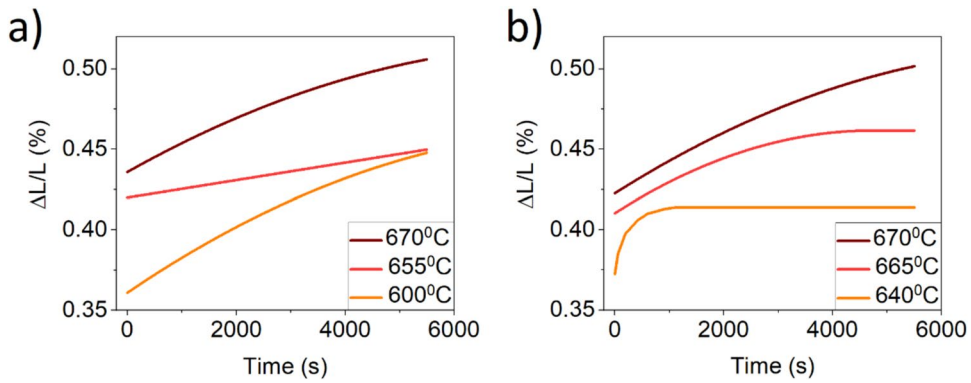

Figure 9 Dilatation curves of microalloyed steel samples with the same solution annealing temperatures and different isothermal transformation temperatures: **a** 0.2HR steel **b** 0.2HR + Cr. The data in **a** and **b** is reproduced from ref 23.

thin-foil samples. For the 0.2HR, 0.2HR + Cr the average inter-sheet distances are 70 and 115 nm, and for 0.4HR, 0.4HR + Cr are 26 and 41 nm, respectively.

The corresponding selected area diffraction patterns (SADPs) of the precipitates are shown in Fig. 12. As found in a previous study on the same steels [23], the presence of rod-shaped VC precipitates lying preferentially along two $(011)_\alpha$ directions was found in steels with 0.4 strain per hot-rolling pass (Fig. 12 a). These VC IP show a $[1\,1\,1]_{VC} \parallel [\,1\,1\,0]_\alpha$ orientation relationship which conforms to the Nishiyama-Wassermann orientation relationship, found also in coarse (⌀ >15 nm) IP[55, 56]. This OR occurs after aging at constant transformation temperatures for relatively large times (over 60 min), where the OR rotates to Nishiyama-Wassermann from the original Baker-Nutting

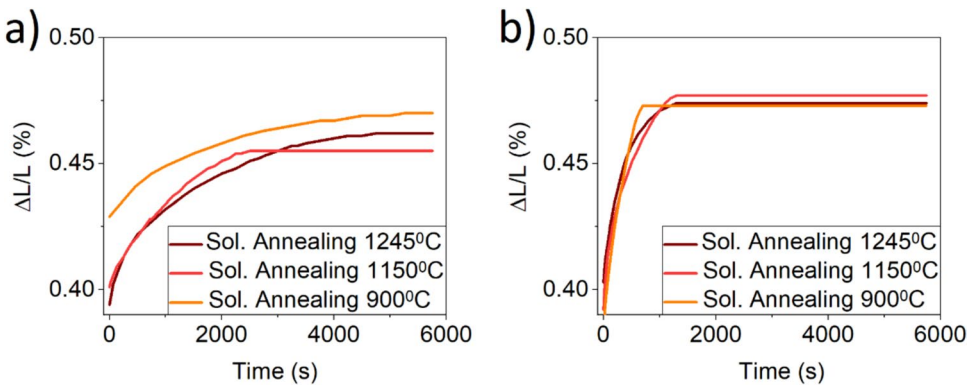

Figure 10 Dilatation curves of microalloyed steel samples with different solution annealing temperatures: **a** 0.4HR steel isothermally transformed at 650˚C, and **b** 0.4HR + Cr isothermally transformed at 660˚C.

orientation relationship [55, 56]. In addition, (V,Mo)C and $(V,Mo)_4C_3$ precipitates were found in the Cr-added steel with 0.4 strain per hot rolling pass (Fig. 12 b)), exhibiting the Baker-Nutting orientation relationships with the ferrite matrix.

The volume fraction and average size of the IP were determined by measuring the area projected of IP on TEM micrographs from carbon extraction replicas. This method is found to yield the same size and distribution as those measured in thin foil samples within experimental error [22, 23]. The precipitate size was obtained using the "analyze particles" tool of the software ImageJ, discarding data registered to be ∅ < 2 nm (indiscernible from noise). The volume fraction was calculated using the Eq. 1 [23], being f_s the percentage area occupied by the IP on a carbon extraction replica image, $\bar{r}$ the average IP radius, and L_{rows} the IP inter-row distance.

$$f_V = f_s \frac{\frac{4}{3}\bar{r}}{L_{rows}} \quad (1)$$

Figure 13 presents the IP volume fraction grouped by diameter ranges from 2 to 30 nm. Comparing steels with the same chemistries with different hot-rolling schedules, it is observed that the increment in strain per pass during the hot-rolling of the V-Mo and Cr-V-Mo microalloyed steels increases the IP volume fraction within the isothermally transformed ferrite. Also, it is found that the volume fraction of the IP ∅ > 20 nm was reduced with the increment in the steels with 0.4 strain per hot-rolling pass, having a more homogeneous distribution of diameters. Figure 14 shows that the average IP volume fraction increases in steels with higher ferrite fraction. In addition, the specimens that were solution annealed at 900 °C have a reduced IP volume fraction. There is no simple conclusion from the analysis of the IP diameter, showing a non-significative reduction in the IP diameter between the Cr-free and the Cr-added steels (for the steels with 0.4 strain per hot-rolling pass). There was no significant change in the IP diameter from changes in the solution annealing temperature ranging from 900 to 1245 °C.

Tensile properties

The engineering stress–strain curves are presented in Fig. 15 a, c, e and g. Figure 15 b, d, f and h gives the yield strength, ultimate tensile strength and elongation from the tensile tests. Contrasting the results of 0.2HR with 0.4HR, and 0.2HR + Cr with 0.4HR + Cr, the increased strain per pass during the hot-rolling produce an increase in all of the strength values (yield and ultimate) and elongation (homogeneous and total). As was reported previously, the Cr addition displaces the maximum values of the mechanical properties by 5–10 °C higher transformation temperature [23]. The current results show no change with different strain per pass during the hot-rolling process. Also, the maximum tensile properties were obtained at solution annealing between 1150 °C for the V-Mo steel, and at 1245 °C for the Cr-V-Mo steel.

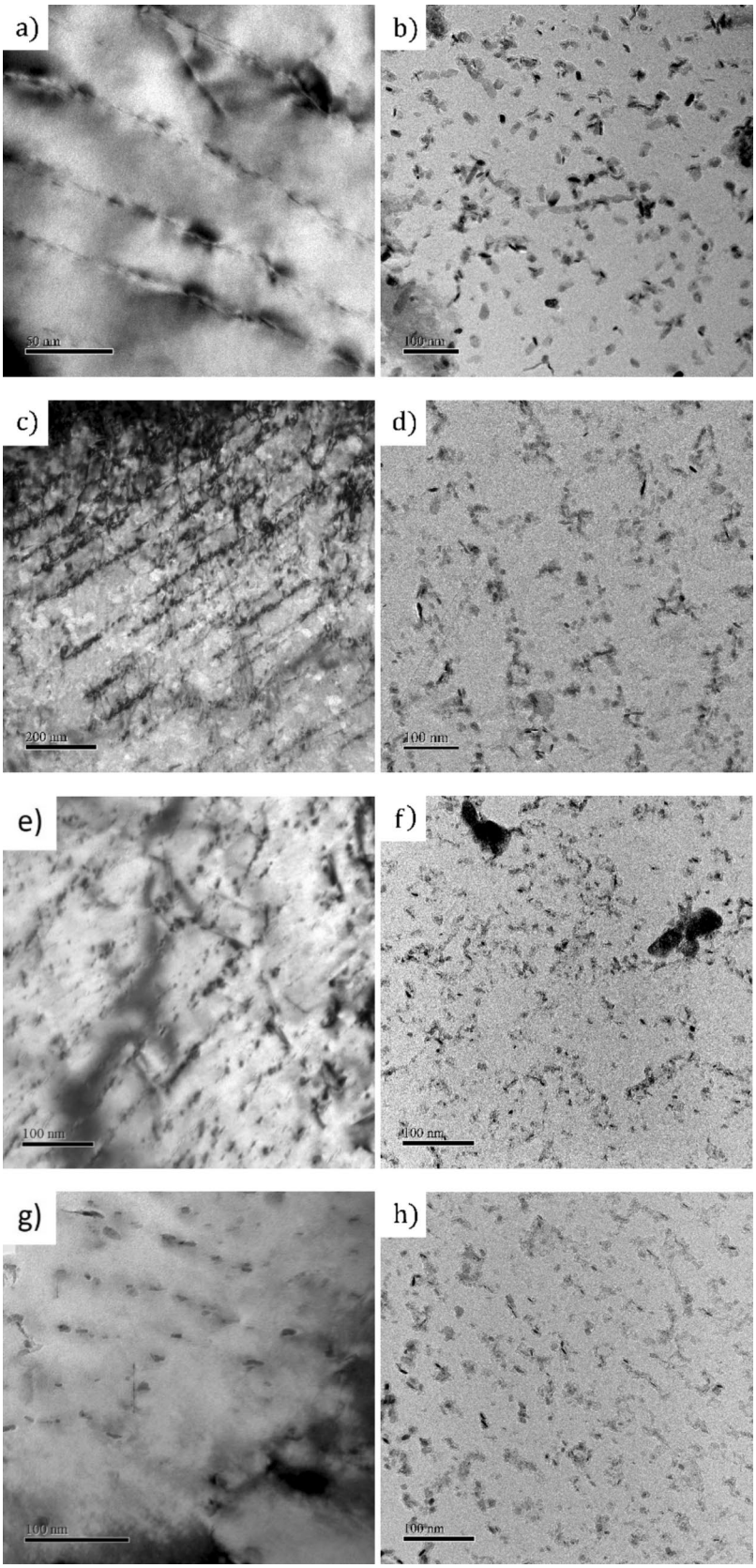

Figure 11 TEM micrographs showing the interphase precipitation distribution (rows) from thin foil samples and their corresponding carbon extraction replica. **a** and **b** 0.2HR steel solution annealed at 1200 °C and isothermal treatment at 650 °C for 90 min. **c** and **d** 0.2HR + Cr steel solution annealed at 1200 °C and isothermal treatment at 660 °C for 90 min. **e** and **f** 0.4HR steel solution annealed at 1150 °C and isothermal treatment at 650 °C for 90 min. **g** and **h** 0.4HR + Cr steel solution annealed at 1245 °C and isothermal treatment at 660 °C for 90 min.

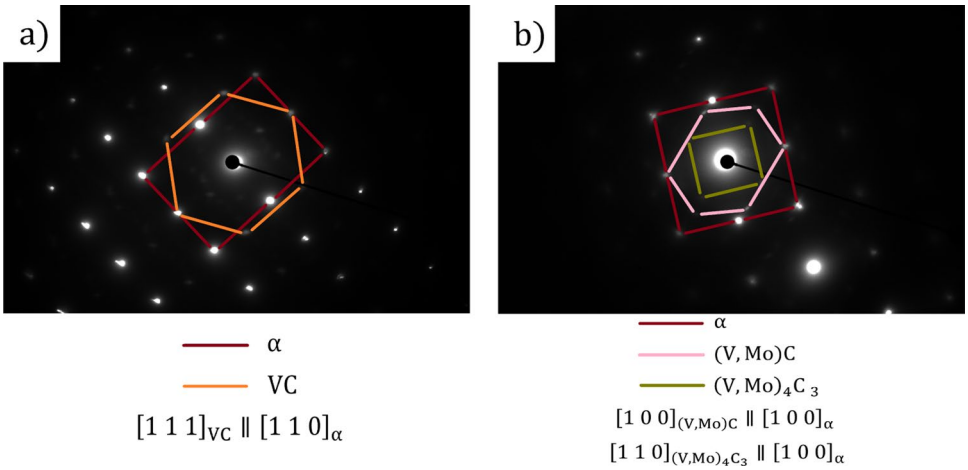

Figure 12 The corresponding diffraction pattern of the IP in the **a** V-Mo steel, and **b** Cr-V-Mo steel.

Discussion

The transformation kinetics of the dual phase structure formed of polygonal ferrite and martensite after the isothermal transformation of V-Mo and Cr-V-Mo was modified by increasing the strain per hot-rolling pass. Moreover, the increased strain per pass during the hot-rolling resulted in a higher volume fraction of ferrite, especially on the Cr-free steel.

All the steels studied contained extensive IP in the ferrite. The character of the $\gamma \rightarrow \alpha$ transformation determines the type and shape of the IP, namely, for example, if the interphase is incoherent then fibrous precipitates are favored [57]. The $\gamma \rightarrow \alpha$ transformation can be decelerated by adding alloying elements such as Mn [58]. In this work, planar IPs were observed, but as the transformation temperature increased above that which gave the maximum ferrite formation, the IP morphology changed to curved IP with irregular sheet spacing (Fig. 16). This is due to the increased diffusion rate at higher transformation temperatures, which reduced the nucleation rate (decreased driving force), and increased the speed of the carbide growth, resulting in larger precipitates with larger interparticle distances.

The increased strain per pass during the hot-rolling resulted in a considerable increment in the volume fraction of fine IP ($\varnothing < 20$ nm). Furthermore, the IP of the V-Mo steel displayed a finer average diameter with a much more homogeneous and narrower size distribution (Fig. 13a and c) in the specimens with higher strain during the hot-rolling. The effect of increased strain per pass was greater than the refining effect of the Cr addition observed in steels with 0.2 strain per pass.

The engineering stress–strain curves (Fig. 15) show the characteristics of a DP steel, such as continuous yielding, and low yield ratio, among others. The continuous yielding behavior is a reflection of the plastic incompatibility between the ferrite and martensite. The ferrite was stressed as a secondary effect of the expansion of the martensite that formatted from the untransformed austenite during the quench after the isothermal transformation [59]. The martensite volume fraction is directly proportional contributor to the DP steel's strengths [1, 59–61]. Additionally, other authors also state that the effect of banded structure usually found in DP steels also affects the mechanical properties [62–64].

Strengthening contributors to the ferrite

In this section, we consider the strength contributions arising from the ferrite, while the contribution from the martensite is given in the next section. The correlation between strength and microstructural constituents has been studied as a function of different strengthening mechanisms. Some models only consider the contributions from within the ferrite as shown in Eq. 2 [65, 66], where $\Delta\sigma_0$ is the lattice friction stress, $\Delta\sigma_{SS}$ is the solid solute strengthening, $\Delta\sigma_{GB}$ is the grain boundary strengthening, $\Delta\sigma_\rho$ is the dislocation strengthening, and $\Delta\sigma_P$ is the precipitation strengthening.

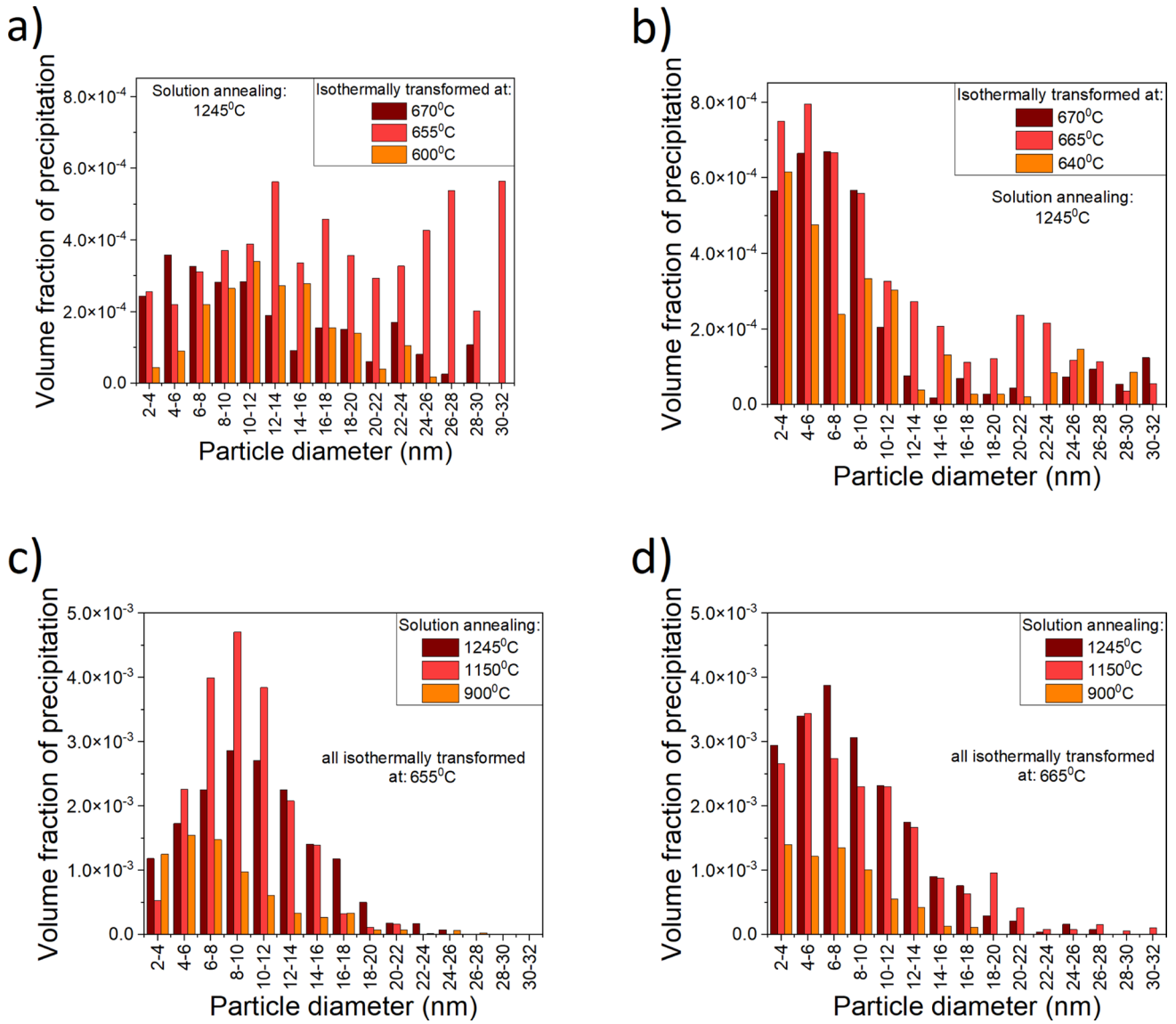

Figure 13 IP size distribution of the interphase precipitation from **a** 0.2HR steel, **b** 0.2HR + Cr steel, **c** 0.4HR steel, **d** 0.4HR + Cr steel. The data in **a** and **b** is reproduced from ref 23.

$$\Delta\sigma_\alpha = \Delta\sigma_0 + \Delta\sigma_{SS} + \Delta\sigma_{GB} + \Delta\sigma_\rho + \Delta\sigma_P \quad (2)$$

Each factor is calculated as follows:

- The Peierls-Nabarro lattice friction stress ($\Delta\sigma_0$) [67]:

$$\sigma_0 = (2G/1-v)\exp(-2\pi w/b) \quad (3)$$

Being G the shear modulus, v the Poisson's ratio, and w the dislocation width and the Burger's vector. Several authors [65, 68] established that the width of an edge dislocation is similar in different steels, using 48 MPa as lattice friction stress in their calculations.

- The solid solution hardening for ferrite ($\Delta\sigma_{SS}$) [7]:

$$\Delta\sigma_{SS} = 4570[C] + 4570[N] + 37[Mn] + 83[Si] + 470[P] + 38[Cu] + 80[Ti] + 0[Ni] - 30[Cr] \quad (4)$$

All the symbols representing the weight percentage of the chemical elements in the ferrite, esti-

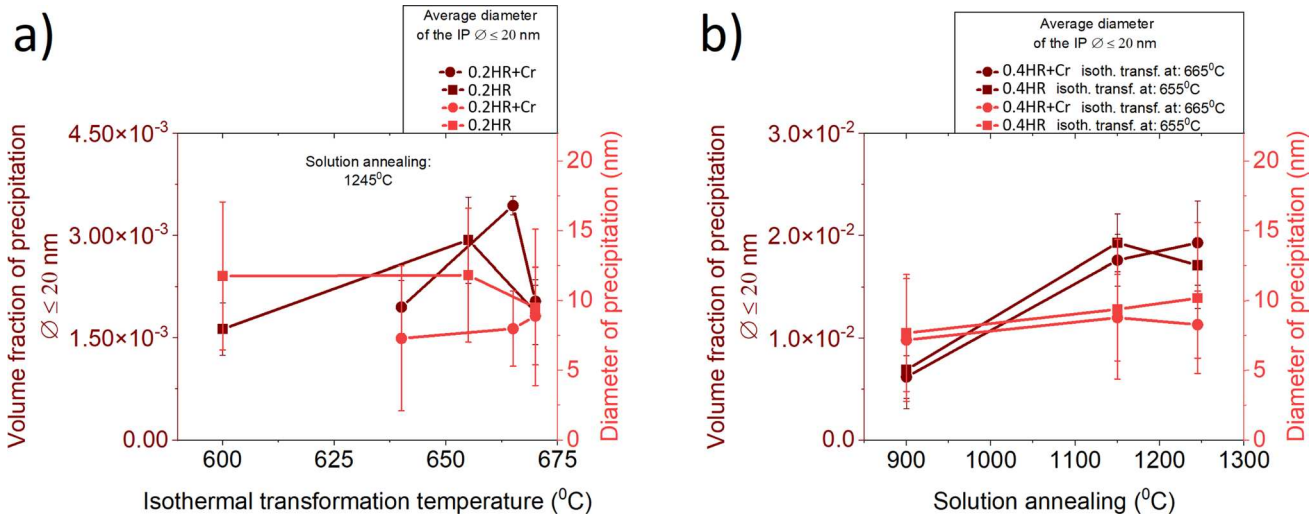

Figure 14 The volume fraction and the average diameter of the interphase precipitation found within the ferrite. The data in a) is reproduced from ref 23.

mated to be the same as Table 1, excluding carbon, which was estimated to be close to its maximum solubility value in ferrite (0.02 wt%).

- The increment in the strength arising from the ferrite grain refinement ($\Delta\sigma_{GB}$) (based on the Hall-Petch relationship) [69–71].

$$\Delta\sigma_{GB} = K_y d_F^{-0.5} \tag{5}$$

Being K_y a constant (0.55 MPa·m$^{0.5}$ for HSLA steel [65, 72, 73]), and d_F the mean grain size measured in m.

- The increment in the yield stress as a result of the dislocation density $(\Delta\sigma_\rho)$ [74]:

$$\Delta\sigma_\rho = \alpha M G b \sqrt{\rho} \tag{6}$$

α is a material constant (0.33 used for DP steels [73]), M is the Taylor factor (2.75 is the average value of random texture bcc metals [73]), G is the shear modulus (80.3 GPa), b is the Burgers vector (2.48×10^{-10} m), and ρ is the dislocation density, which was measured from TEM pictures of the ferrite isothermally transformed, obtaining values between 5.6×10^{13} and 6.9×10^{13} m^{-2}.

- And finally, the contribution of precipitation to the yield strength can be calculated using the Ashby-Orowan model [75, 76]:

$$\Delta\sigma_P = 8995 * \frac{f_V^{1/2}}{d} \ln(2.417d) \tag{7}$$

Where f_V is the volume fraction of the IP, and d is the average diameter of the IP in nanometers. In this investigation, these calculations have been undertaken with the IP $\emptyset < 20\ nm$. As with other investigations [22, 23], relatively large precipitates $(\emptyset > 20\ nm)$ were not included in the calculation because they do not contribute to hardening, but have a strong influence on the volume fraction data, thereby distorting the output of the model.

Kang's model [13, 68] is also widely used to predict the yield strength in DP steels. This model is a root-mean-square model which includes all the parameters described above, except the precipitation contribution, and also includes a factor dependent on the volume fraction of martensite. These are major issues when the calculation of the yield strength needs to be done, especially because the IP represents an important contributor to the total yield strength of microalloyed steels [22, 23], and also because the parameter which includes the martensite volume fraction is insignificant compared to the rest of the contributors.

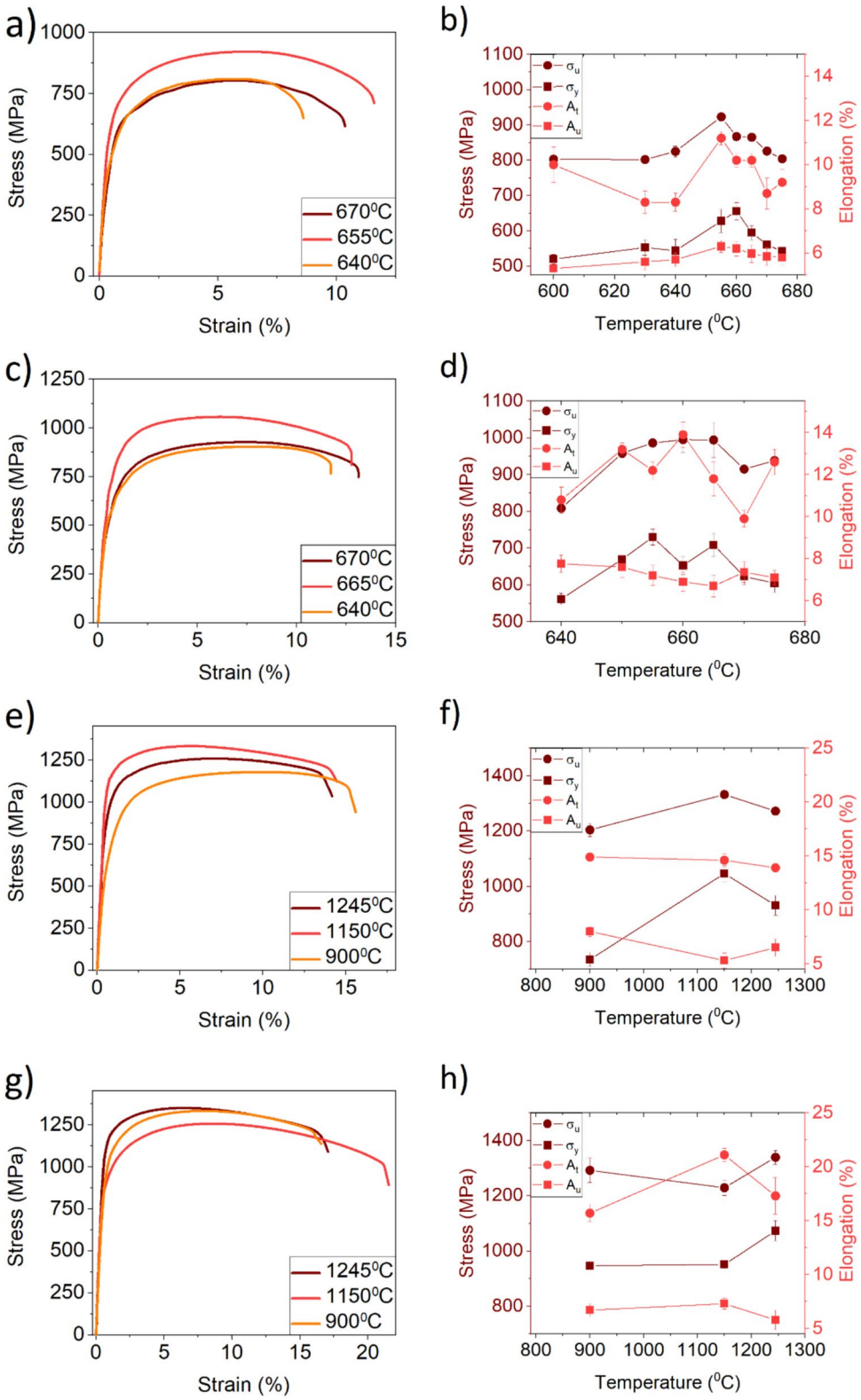

Figure 15 The engineering strain–stress curves of **a** 0.2HR steel, **c** 0.2HR + Cr steel, **e** 0.4HR steel, and **g** 0.4HR + Cr steel. Yield strength, tensile strength and total elongation as a function of the isothermal transformation temperature for **b** 0.2HR steel, **d** 0.2HR + Cr steel, **f** 0.4HR steel, and **h** 0.4HR + Cr steel. s_y is the yield strength, s_u is the ultimate tensile strength, A_t is the total elongation, and A_u is the homogeneous elongation. The data in **a**, **b**, **c**, and **d** is reproduced from ref 23.

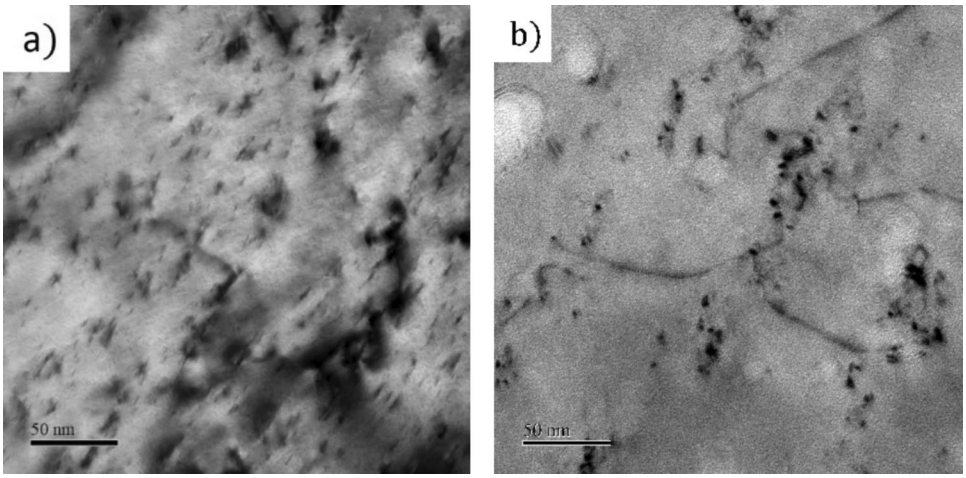

Figure 16 TEM-thin foil micrograph of the evolution of IP's morphology with the isothermal temperature in V-Mo microalloyed steel, 0.2 strain during hot rolling, solution annealed at 1200˚C and isothermal holding at **a** 665˚C for 90 min, and **b** 675˚C for 90 min.

Strengthening contributors to the martensite

The 0.2% proof strength is a function of multiple characteristics of the martensite in DP steels, such as the carbon content [63]. Other factors of martensite can be considered, such as packet size and the orientation of them, but it has also been demonstrated that martensitic structures with equiaxed grains are obtained when the holding times are above 900 °C [63].

The yield strength of martensite, $\Delta\sigma_{\alpha'}$, was calculated based on the exponential law developed by Pierman et al. [63], Eq. 8, for the calculation of the strength contribution from martensite in DP steels. This term was determined from experimental results observed on multiple bulk martensitic steels but also fitting with experimental results of several grades of DP steels [62–64].

$$\Delta\sigma_{\alpha'} = \sigma_{y_{0,\alpha'}} + k_{\alpha'}\left(1 - \exp\left(-\varepsilon_p n_{\alpha'}\right)\right) \tag{8}$$

here $\sigma_{y_{0,\alpha'}}$, $k_{\alpha'}$, ε_p, and $n_{\alpha'}$ are the current yield strength, the hardening modulus, the accumulated plastic strain, and the hardening exponent, respectively. This expression presumed the Young's modulus for ferrite and martensite are the same and set $E = 120$ GPa and $v = 0.3$.

The initial yield stress $\sigma_{y_{0,\alpha'}}$ is given principally by the action of carbon in the martensite, where $C_{\alpha'}$ is the wt.% of carbon in the martensite. The amount of carbon in martensite is equal to the total carbon of the steel (wt.%) minus the volumetric fraction of ferrite multiplied by 0.02%, which is the maximum solubility of carbon in ferrite. The solubility of carbon in ferrite reduces as the temperature decreases, but the value of 0.02% in solution is at the eutectoid temperature which is close to the temperature at which isothermal transformation took place. During the $\gamma \rightarrow \alpha$ transformation, carbon does not migrate fast enough to the martensite but is tied up in the interphase precipitation [25].

$$\sigma_{y_{0,\alpha'}} = 300 + 1000\left(C_{\alpha'}\right)^{1/3} \tag{9}$$

The hardening modulus $k_{\alpha'}$[64]:

$$k_{\alpha'} = \frac{1}{n_{\alpha'}}\left[a + \frac{bC_{\alpha'}}{1 + \left(\frac{C_{\alpha'}}{C_0}\right)^q}\right] \tag{10}$$

With a hardening exponent $n_{\alpha'} = 120$, $a = 33GPa$, $b = 360GPa$, $C_0 = 0.7$ and $q = 1.45$.

Banding effect and the combined effect of the phases on the yield strength

In literature, there are multiple models describing the banding effect and how the mechanical properties are dependent on it. From optical micrography, one main feature that can be taken to characterize the banding effect on dual-phase steels is the aspect ratio of the bands [62]. In this study, a general aspect ratio was taken for each sample (considering both phases), averaging the number of intersections of a square grid with the ferrite/martensite interphase in optical micrographs as undertaken by ref [62]. The aspect ratio is defined as the ratio between the number of intersections in the rolling direction to the average intersection in the normal direction. Ramazani et al. [62] stated that aspect ratios of

Table 3 Aspect ratio and calculations of the different contributors to the yield strength of the DP microalloyed steels

Steel	Reaustenitization [°C]	T_{iso} [°C]	$\Delta\sigma_{\alpha}$[MPa]	$\Delta\sigma_{\alpha'}$[MPa]	AR	Experimental YS [MPa]	Calculated YS (σ_y) [MPa]
0.2HR	1245	600	632	1203	0.67	520	562
	1245	655	676	1261	0.79	630	672
	1245	670	670	1181	0.61	560	530
0.2HR + Cr	1245	640	677	1183	0.71	563	606
	1245	665	720	1514	0.85	710	702
	1245	670	676	1420	0.72	620	578
0.4HR	900	650	873	1395	0.71	735	688
	1150	650	980	1493	~1	1046	1051
	1245	650	886	1556	~1	931	963
0.4HR + Cr	900	660	833	1325	0.94	947	866
	1150	660	930	1401	0.91	951	907.4
	1245	660	945	1556	~1	1073	1002

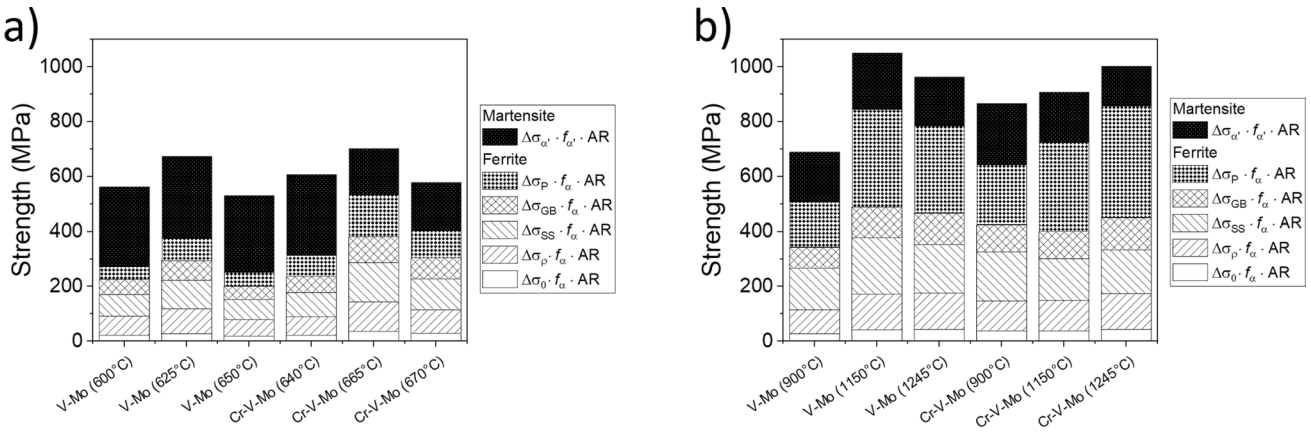

Figure 17 Yield strength contributors of DP V-Mo and Cr-V-Mo microalloyed steels **a** deformed at a strain of 0.2 during the hot-rolling, solution annealed at 1245°C and isothermally transformed at different temperatures. **b** deformed at a strain of 0.4 during the hot-rolling, solution annealed at different temperatures and isothermally transformed at 650 °C (V-Mo) and 660 °C (Cr-V-Mo).

around 1 can be considered as equiaxed structures, but values higher than 1 are banded structures. Measurements of the aspect ratio were made, and the results are presented in Table 3.

In this study, a combined model is presented to predict the yield strength of the DP microalloyed steels. Equation 6 presents the total yield strength σ_y as the sum of the contribution of each microconstituent, multiplied by the volume fraction of each one, and the total multiplied by the inverse of the aspect ratio (AR) related to the banding effect. The results are presented in Table 3, from the presented model, which match the experimental results of the different DP microalloyed steels studied within an error band of 10%. Figure 17 gives the different contributions to the strength arising from the different microstructural constituents. This clearly shows that the increased strain per pass during hot-rolling increased the precipitation hardening within the ferrite.

$$\sigma_y = \left(\Delta\sigma_{\alpha} \cdot f_{\alpha} + \Delta\sigma_{\alpha'} \cdot f_{\alpha'}\right) \cdot \left(\frac{1}{AR}\right) \tag{11}$$

Conclusions

The effect of increased strain per pass during the hot-rolling and changes in the solution annealing on the mechanical properties of V-Mo and Cr-V-Mo dual-phase (DP) microalloyed steels were studied, concluding that:

1. A dual-phase microstructure of ferrite and martensite was produced by isothermally transformed V-Mo and Cr-V-Mo steels. A higher strain during the hot-rolling accelerated the transformation kinetics, and as a result the volume fraction of ferrite increases in expense of the martensite.
2. The V-Mo and Cr-V-Mo steels with both 0.2 and 0.4 strain per pass during the hot rolling have a relatively large effect on the interphase precipitation within the ferrite. The increased strain per pass produces a higher volume fraction of interphase precipitation in the ferrite, increasing the precipitation contribution to the yield strength of dual-phase microalloyed steels.
3. The best combination of tensile properties in the V-Mo and Cr-V-Mo steels was obtained at high solution-annealing temperatures, at a temperature just below that at which the abnormal growth of the prior-austenite grains occurred. In the V-Mo steel, the optimum solution annealing was 1150 °C, after that, the contributions by the ferrite grain size, the dislocation density, and the precipitation strengthening were reduced. Furthermore, holding at a low solution annealing temperature was not beneficial, reducing the mechanical properties and increasing the banding effect.
4. All the microconstituents contribute significantly to the mechanical properties of the dual-phase microalloyed steels. A new model for calculating the yield strength of dual-phase (ferrite + martensite) microalloyed steels was introduced, including the effect of the most relevant contributors from the phases. This gave an excellent match between the model and results from experiments.

Acknowledgements

The authors wish to thank Neville and Eileen Baker Charitable Trust for the scholarship of Karol F. Rodriguez-Galeano. The authors also want to thank the Henry Royce Institute for Advanced Materials, funded through EPSRC grants EP/R00661X/1, EP/S019367/1 for access to the JEOL JEM-F200 through Royce@Sheffield.

Author contributions

K Rodriguez-Galeano undertook the research and drafted the manuscript. J. Nutter helped with the electron microscopy, Y. Azakli assisted in making the steel melts and C. Slater assisted with the thermomechanical processing of the steel. W. Mark Rainforth conceived the project, provided critical interpretation and assisted with writing the manuscript.

Data and code availability

Not applicable.

Declarations

Conflict of interest On behalf of all authors, the corresponding author states that there is no conflict of interest.

Ethical approval Not applicable.

References

[1] Davies RG (1978) Influence of martensite composition and content on the properties of dual phase steels. Metall Trans A 9:671–679. https://doi.org/10.1007/BF02659924

[2] Oliver S, Jones TB, Fourlaris G (2007) Dual phase versus TRIP strip steels: comparison of dynamic properties for automotive crash performance. Mater Sci Technol 23:423–431. https://doi.org/10.1179/174328407X168937

[3] Tasan CC, Diehl M, Yan D et al (2015) An overview of dual-phase steels: advances in microstructure-oriented processing and micromechanically guided design. Annu Rev Mater Res 45:391–431. https://doi.org/10.1146/annurev-matsci-070214-021103

[4] Speich G, Miller R (1979) Mechanical properties of ferrite-martensite steels. Struct Prop Dual-Phase Steels 1979:145–182

[5] Marder AR (1982) Deformation characteristics of dual-phase steels. Metall Trans A, Phys Metall Mater Sci 13A:85–92. https://doi.org/10.1007/BF02642418

[6] Chen HC, Cheng GH (1989) Effect of martensite strength on the tensile strength of dual phase steels. J Mater Sci 24:1991–1994. https://doi.org/10.1007/BF02385411

[7] Yong QL, Ma MT, Wu BR (1989) Microalloyed steel-physical and mechanical metallurgy. Mech Eng Press, Beijing

[8] Funakawa Y, Shiozaki T, Tomita K et al (2004) Development of high strength hot-rolled sheet steel consisting of ferrite and nanometer-sized carbides. ISIJ Int 44:1945–1951. https://doi.org/10.2355/isijinternational.44.1945

[9] Cong ZH, Jia N, Sun X et al (2009) Stress and strain partitioning of ferrite and martensite during deformation. Metall Mater Trans A Phys Metall Mater Sci 40:1383–1387. https://doi.org/10.1007/s11661-009-9824-2

[10] Charleux M, Poole WJ, Militzer M, Deschamps A (2001) Precipitation behavior and its effect on strengthening of an HSLA-Nb/Ti steel. Metall Mater Trans A Phys Metall Mater Sci 32:1635–1647. https://doi.org/10.1007/s11661-001-0142-6

[11] Park DB, Huh MY, Shim JH et al (2013) Strengthening mechanism of hot rolled Ti and Nb microalloyed HSLA steels containing Mo and W with various coiling temperature. Mater Sci Eng A 560:528–534. https://doi.org/10.1016/j.msea.2012.09.098

[12] Tamura I, Tanaka T, Sekine H (1988) Thermomechanical processing of high-strength low-alloy steels. Butterworth-Heinemann, London

[13] Kestenbach HJ, Campos SS, Morales EV (2006) Role of interphase precipitation in microalloyed hot strip steels. Mater Sci Technol 22:615–626. https://doi.org/10.1179/026708306X81487

[14] DeArdo AJ, Hua MJ, Cho KG, Garcia CI (2009) On strength of microalloyed steels: an interpretive review. Mater Sci Technol 25:1074–1082. https://doi.org/10.1179/174328409X455233

[15] Ouchi C (2001) Development of steel plates by intensive use of TMCP and direct quenching processes. ISIJ Int 41:542–553. https://doi.org/10.2355/isijinternational.41.542

[16] Vervynckt S, Verbeken K, Lopez B, Jonas JJ (2012) Modern HSLA steels and role of non-recrystallisation temperature. Int Mater Rev 57:187–207. https://doi.org/10.1179/1743280411Y.0000000013

[17] Siwecki T (1992) Modelling of microstructure evolution during recrystallization controlled rolling. ISIJ Int 32:368–376. https://doi.org/10.2355/isijinternational.32.368

[18] Militzer M, Hawbolt EB, Meadowcroft TR (2000) Microstructural model for hot strip rolling of high-strength low-alloy steels. Metall Mater Trans A Phys Metall Mater Sci 31:1247–1259. https://doi.org/10.1007/s11661-000-0120-4

[19] Hanlon DN, Sietsma J, Van Der Zwaag S (2001) The effect of plastic deformation of austenite on the kinetics of subsequent ferrite formation. ISIJ Int 41:1028–1036. https://doi.org/10.2355/isijinternational.41.1028

[20] Calvo J, Jung IH, Elwazri AM et al (2009) Influence of the chemical composition on transformation behaviour of low carbon microalloyed steels. Mater Sci Eng A 520:90–96. https://doi.org/10.1016/j.msea.2009.05.027

[21] Lanzagorta JL, Jorge-Badiola D, Gutiérrez I (2010) Effect of the strain reversal on austenite-ferrite phase transformation in a Nb-microalloyed steel. Mater Sci Eng A 527:934–940. https://doi.org/10.1016/j.msea.2009.09.007

[22] Gong P, Liu XG, Rijkenberg A, Rainforth WM (2018) The effect of molybdenum on interphase precipitation and microstructures in microalloyed steels containing titanium and vanadium. Acta Mater 161:374–387. https://doi.org/10.1016/j.actamat.2018.09.008

[23] Rodriguez-Galeano KF, Nutter J, Azakli Y et al (2024) Influence of Cr and Cr+Nb on the interphase precipitation and mechanical properties of V-Mo microalloyed steels. Mater Sci Eng A 893:146140. https://doi.org/10.1016/j.msea.2024.146140

[24] Lu J, Omotoso O, Wiskel JB et al (2012) Strengthening mechanisms and their relative contributions to the yield strength of microalloyed steels. Metall Mater Trans A Phys Metall Mater Sci 43:3043–3061. https://doi.org/10.1007/s11661-012-1135-3

[25] Tsai SP, Jen CH, Yen HW et al (2017) Effects of interphase TiC precipitates on tensile properties and dislocation structures in a dual phase steel. Mater Charact 123:153–158. https://doi.org/10.1016/j.matchar.2016.11.023

[26] Snieder G, Kerr HW (1984) Effects of chromium additions and flux type on the structure and properties of HSLA steel submerged arc weld metal. Can Metall Q 23:315–325. https://doi.org/10.1179/cmq.1984.23.3.315

[27] Jorge JCF, Souza LFG, Rebello JMA (2001) The effect of chromium on the microstructure/toughness relationship of C-Mn weld metal deposits. Mater Charact 47:195–205. https://doi.org/10.1016/S1044-5803(01)00168-1

[28] Xu S, Cao R, Gao J et al (2024) Effect of Cr on the phase transformation and interphase nanoprecipitation behaviours of high-strength microalloyed steels. Mater Charact 207:113504. https://doi.org/10.1016/j.matchar.2023.113504

[29] Fadel A, Glišić D, Radović N, Drobnjak D (2012) Influence of Cr, Mn and mo addition on structure and properties of V microalloyed medium carbon steels. J Mater Sci Technol 28:1053–1058. https://doi.org/10.1016/S1005-0302(12)60172-8

[30] Avazkonandeh-Gharavol MH, Haddad-Sabzevar M, Haerian A (2009) Effect of chromium content on the microstructure and mechanical properties of multipass MMA, low alloy steel weld metal. J Mater Sci 44:186–197. https://doi.org/10.1007/s10853-008-3103-2

[31] Jorge JCF, Monteiro JLD, Gomes AJDC et al (2019) Influence of welding procedure and PWHT on HSLA steel weld metals. J Mater Res Technol 8:561–571. https://doi.org/10.1016/j.jmrt.2018.05.007

[32] Zhang J, Wang FM, Yang ZB, Li CR (2016) Microstructure, precipitation, and mechanical properties of V-N-alloyed steel after different cooling processes. Metall Mater Trans A Phys Metall Mater Sci 47:6621–6631. https://doi.org/10.1007/s11661-016-3763-5

[33] Mirzadeh H, Alibeyki M, Najafi M (2017) Unraveling the initial microstructure effects on mechanical properties and work-hardening capacity of dual-phase steel. Metall Mater Trans A Phys Metall Mater Sci 48:4565–4573. https://doi.org/10.1007/s11661-017-4246-z

[34] Shen XJ, Tang S, Wu YJ et al (2017) Evolution of microstructure and crystallographic texture of microalloyed steel during warm rolling in dual phase region and their influence on mechanical properties. Mater Sci Eng A 685:194–204. https://doi.org/10.1016/j.msea.2016.12.108

[35] Xue J, Zhao Z, Bin C et al (2019) Effects of rolling and coiling temperature on the microstructure and mechanical properties of hot-rolled high strength complex phase steel. Mater Res Express. https://doi.org/10.1088/2053-1591/ab1404

[36] Ahmad E, Priestner R (1998) Effect of rolling in the intercritical region on the tensile properties of dual-phase steel. J Mater Eng Perform 7:772–776. https://doi.org/10.1361/105994998770347341

[37] Kolbasnikov NG, Bezobrazov YA, Naumov AA (2013) Structural evolution of high-strength dual-phase steel in hot rolling. Steel Transl 43:455–459. https://doi.org/10.3103/S0967091213070085

[38] Zhang K, Li Z, Wang Z et al (2016) Precipitation behavior and mechanical properties of hot-rolled high strength Ti-Mo-bearing ferritic sheet steel: the great potential of nanometer-sized (Ti, Mo)C carbide. J Mater Res 31:1254–1263. https://doi.org/10.1557/jmr.2016.154

[39] Davenport AT, Berry FG, Honeycombe RWK et al (1968) Interphase precipitation in iron alloys interphase precipitation in iron alloys. Met Sci J 2(1):104–106. https://doi.org/10.1179/030634568790443341

[40] Davenport AT, Honeycombe RWK (1971) Precipitation of carbides at γ -α boundaries in alloy steels. Proc R Soc Lond A Math Phys Sci 322:191–205

[41] Honeycombe RWK (1985) Fundamental aspects of precipitation in microalloyed steels. HSLA Steels: Metallurgy and Applications. 1985:243–250

[42] Zhang YJ, Miyamoto G, Shinbo K, Furuhara T (2013) Effects of α/γ orientation relationship on VC interphase precipitation in low-carbon steels. Scr Mater 69:17–20. https://doi.org/10.1016/j.scriptamat.2013.03.020

[43] Zhang YJ, Chandiran E, Dong HK et al (2021) Current understanding of microstructure and properties of micro-alloyed low carbon steels strengthened by interphase precipitation of nano-sized alloy carbides: a review. Jom 73:3214–3227. https://doi.org/10.1007/s11837-021-04882-w

[44] Zhang YJ, Miyamoto G, Shinbo K, Furuhara T (2017) Quantitative measurements of phase equilibria at migrating α/γ interface and dispersion of VC interphase precipitates: Evaluation of driving force for interphase precipitation. Acta Mater 128:166–175. https://doi.org/10.1016/j.actamat.2017.02.020

[45] Yen HW, Chen PY, Huang CY, Yang JR (2011) Interphase precipitation of nanometer-sized carbides in a titanium-molybdenum-bearing low-carbon steel. Acta Mater 59:6264–6274. https://doi.org/10.1016/j.actamat.2011.06.037

[46] Zhang YJ, Miyamoto G, Shinbo K et al (2015) Effects of transformation temperature on VC interphase precipitation and resultant hardness in low-carbon steels. Acta Mater 84:375–384. https://doi.org/10.1016/j.actamat.2014.10.049

[47] Rodriguez-Galeano KF, Romano-Acosta LF, Palmiere EJ, Rainforth WM (2023) A new approach to etching low-carbon microalloyed steels to reveal prior austenite grain

boundaries and the dual-phase microstructure. J Microsc 289:73–79. https://doi.org/10.1111/jmi.13153

[48] Bengochea R, López B, Gutierrez I (1998) Microstructural evolution during the austenite-to-ferrite transformation from deformed austenite. Metall Mater Trans A Phys Metall Mater Sci 29:417–426. https://doi.org/10.1007/s11661-998-0122-1

[49] Bengochea R, López B, Gutierrez I (1999) Influence of the prior austenite microstructure on the transformation products obtained for C-Mn-Nb steels after continuous cooling. ISIJ Int 39:583–591. https://doi.org/10.2355/isijinternational.39.583

[50] Zhao H, Palmiere EJ (2018) Effect of austenite grain size on acicular ferrite transformation in a HSLA steel. Mater Charact 145:479–489. https://doi.org/10.1016/j.matchar.2018.09.013

[51] Yang Y, Zhan D, Lei H et al (2020) Coupling effect of prior austenite grain size and inclusion characteristics on acicular ferrite formation in Ti-Zr deoxidized low carbon steel. Metall Mater Trans B Process Metall Mater Process Sci 51:480–491. https://doi.org/10.1007/s11663-020-01785-0

[52] Wang Q, Zou X, Matsuura H, Wang C (2018) Evolution of inclusions during the 1473 K (1200 °C) heating process of EH36 shipbuilding steel. Metall Mater Trans B Process Metall Mater Process Sci 49:18–22. https://doi.org/10.1007/s11663-017-1133-3

[53] Jin HH, Shim JH, Cho YW, Lee HC (2003) Formation of intragranular acicular ferrite grains in a Ti-containing low carbon steel. ISIJ Int 43:1111–1113. https://doi.org/10.2355/isijinternational.43.1111

[54] Li M, Matsuura H, Tsukihashi F (2019) Time-dependent evolution of Ti-bearing oxide inclusions during isothermal holding at 1573 K (1300 °C). Metall Mater Trans A Phys Metall Mater Sci 50:863–873. https://doi.org/10.1007/s11661-018-5015-3

[55] Yen HW, Chen CY, Wang TY et al (2010) Orientation relationship transition of nanometre sized interphase precipitated TiC carbides in Ti bearing steel. Mater Sci Technol 26:421–430. https://doi.org/10.1179/026708309X12512744154207

[56] Law NC, Parsons SA, Howell PR, Edmonds DV (1987) Crystallography of carbide precipitation at transformation interfaces during austenite decomposition in a low-alloy steel. Mater Sci Technol (United Kingdom) 3:642–648. https://doi.org/10.1179/mst.1987.3.8.642

[57] Edmonds DV (1972) Occurrence of fibrous VC during transformation of an Fe-V-C steel. J Iron Steel Inst 210:363–365

[58] Khalid F, a., Edmonds D V. (1993) Interphase precipitation in microalloyed engineering steels and model alloy. Mater Sci Technol 9:384–396. https://doi.org/10.1179/026708393790350468

[59] Sakaki T, Sugimoto K, Fukuzato T (1983) Role of internal stress for continuous yielding of dual-phase steels. Acta Metall 31:1737–1746. https://doi.org/10.1016/0001-6160(83)90172-4

[60] Mazinani M, Poole WJ (2007) Effect of martensite plasticity on the deformation behavior of a low-carbon dual-phase steel. Metall Mater Trans A Phys Metall Mater Sci 38:328–339. https://doi.org/10.1007/s11661-006-9023-3

[61] Peng-Heng C, Preban AG (1985) The effect of ferrite grain size and martensite volume fraction on the tensile properties of dual phase steel. Acta Metall 33:897–903. https://doi.org/10.1016/0001-6160(85)90114-2

[62] Ramazani A, Mukherjee K, Prahl U, Bleck W (2012) Modelling the effect of microstructural banding on the flow curve behaviour of dual-phase (DP) steels. Comput Mater Sci 52:46–54. https://doi.org/10.1016/j.commatsci.2011.05.041

[63] Pierman AP, Bouaziz O, Pardoen T et al (2014) The influence of microstructure and composition on the plastic behaviour of dual-phase steels. Acta Mater 73:298–311. https://doi.org/10.1016/j.actamat.2014.04.015

[64] Lai Q, Brassart L, Bouaziz O et al (2016) Influence of martensite volume fraction and hardness on the plastic behavior of dual-phase steels: Experiments and micromechanical modeling. Int J Plast 80:187–203. https://doi.org/10.1016/j.ijplas.2015.09.006

[65] Mao X, Huo X, Sun X, Chai Y (2010) Strengthening mechanisms of a new 700 MPa hot rolled Ti-microalloyed steel produced by compact strip production. J Mater Process Technol 210:1660–1666. https://doi.org/10.1016/j.jmatprotec.2010.05.018

[66] Kamikawa N, Abe Y, Miyamoto G et al (2014) Tensile behavior of Ti, Mo-added low carbon steels with interphase precipitation. ISIJ Int 54:212–221. https://doi.org/10.2355/isijinternational.54.474

[67] Soboyejo W (2002) Mechanical properties of engineered materials. CRC Press

[68] Kang YL, Han QH, Zhao XM, Cai MH (2013) Influence of nanoparticle reinforcements on the strengthening mechanisms of an ultrafine-grained dual phase steel containing titanium. Mater Des 44:331–339. https://doi.org/10.1016/j.matdes.2012.07.068

[69] Hall EO (1951) The deformation and ageing of mild steel: II characteristics of the Lüders deformation. Proc Phys Soc Sect B 64:742–747. https://doi.org/10.1088/0370-1301/64/9/302

[70] Eo HALL (1954) Variation of hardness of metals with grain size. Nature 173:948–949

[71] Petch NJ (1953) The cleavage strength of polycrystals. I Iron Steel Inst 174:25–28
[72] Mazaheri Y, Kermanpur A, Najafizadeh A (2015) Strengthening mechanisms of ultrafine grained dual phase steels developed by new thermomechanical processing. ISIJ Int 55:218–226. https://doi.org/10.2355/isijinternational.55.218
[73] Bailey JE, Hirsch PB (1960) The dislocation distribution flow stress and stored energy in cold worked crystalline silver. Philos Mag 5(53):485–497
[74] Chin GY, Mammel WL (1967) Computer solutions of Taylor analysis for axisymmetric flow. Trans Metall Soc AIME 239(9):1400
[75] Gladman T (1997) The physical metallurgy of microalloyed steels. The Institute of Materials, London
[76] Gladman T (1999) Precipitation hardening in metals. Mater Sci Technol 15(1):30–36. https://doi.org/10.1007/978-1-4615-8723-1_23